

# Structure-tunable supraparticle assemblies of hollow cupric oxide sheathed with nanographenes

*Minsu Gu,<sup>†1</sup> Woo-ram Lee,<sup>†2</sup> Minkyung Kim,<sup>3</sup> Jiwoong Kang,<sup>2</sup> Jae Sung Lee,<sup>3</sup> Levi T. Thompson,<sup>4</sup>  
and Byeong-Su Kim<sup>1\*</sup>*

<sup>1</sup>Department of Chemistry, Yonsei University, Seoul 03722, Korea

<sup>2</sup>Department of Chemical Engineering, University of Michigan, Ann Arbor, Michigan 48109,  
United States

<sup>3</sup>School of Energy and Chemical Engineering, Ulsan National Institute of Science and  
Technology (UNIST), Ulsan 44919, Korea

<sup>4</sup>College of Engineering, University of Delaware, Newark, Delaware 19716, United States

<sup>†</sup>These authors contributed equally to this work.

E-mail: bskim19@yonsei.ac.kr (B.-S.K.)

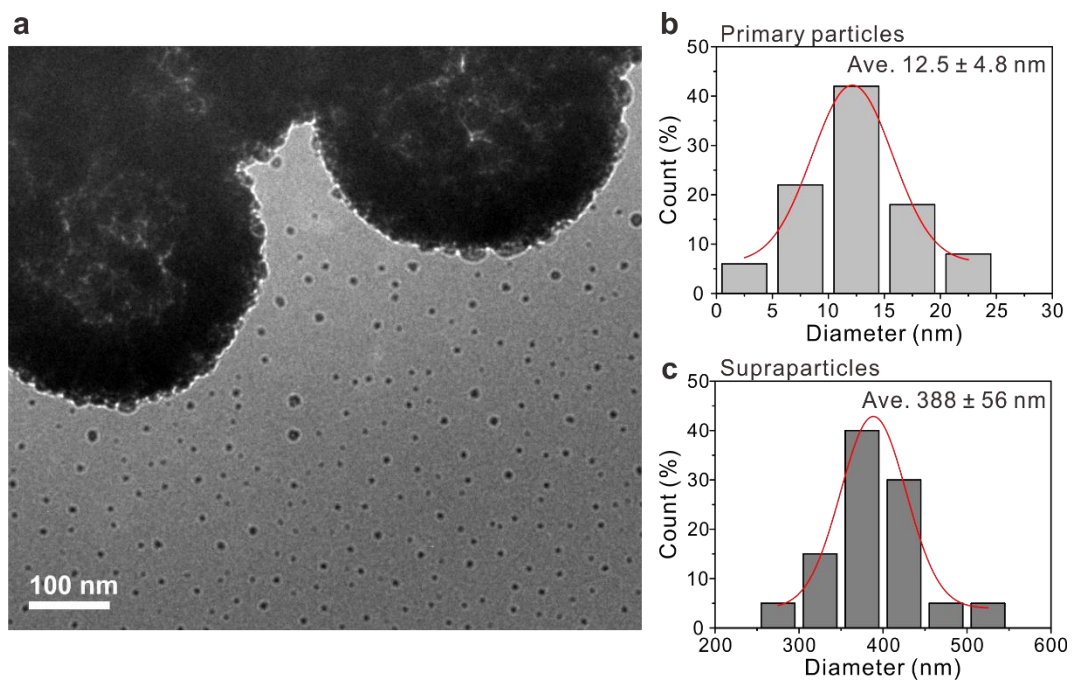


**Figure S1.** (a) TEM image of hollow Cu<sub>2</sub>O SPs with the corresponding size distribution histograms of Cu<sub>2</sub>O for (b) primary particles and (c) supraparticles (SPs).

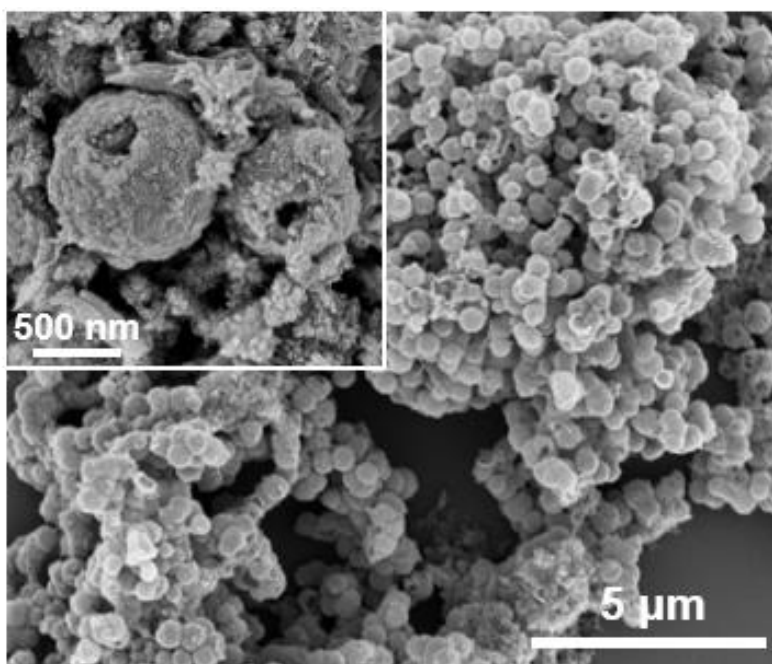


**Figure S2.** SEM images of NGO coated Cu<sub>2</sub>O SPs.

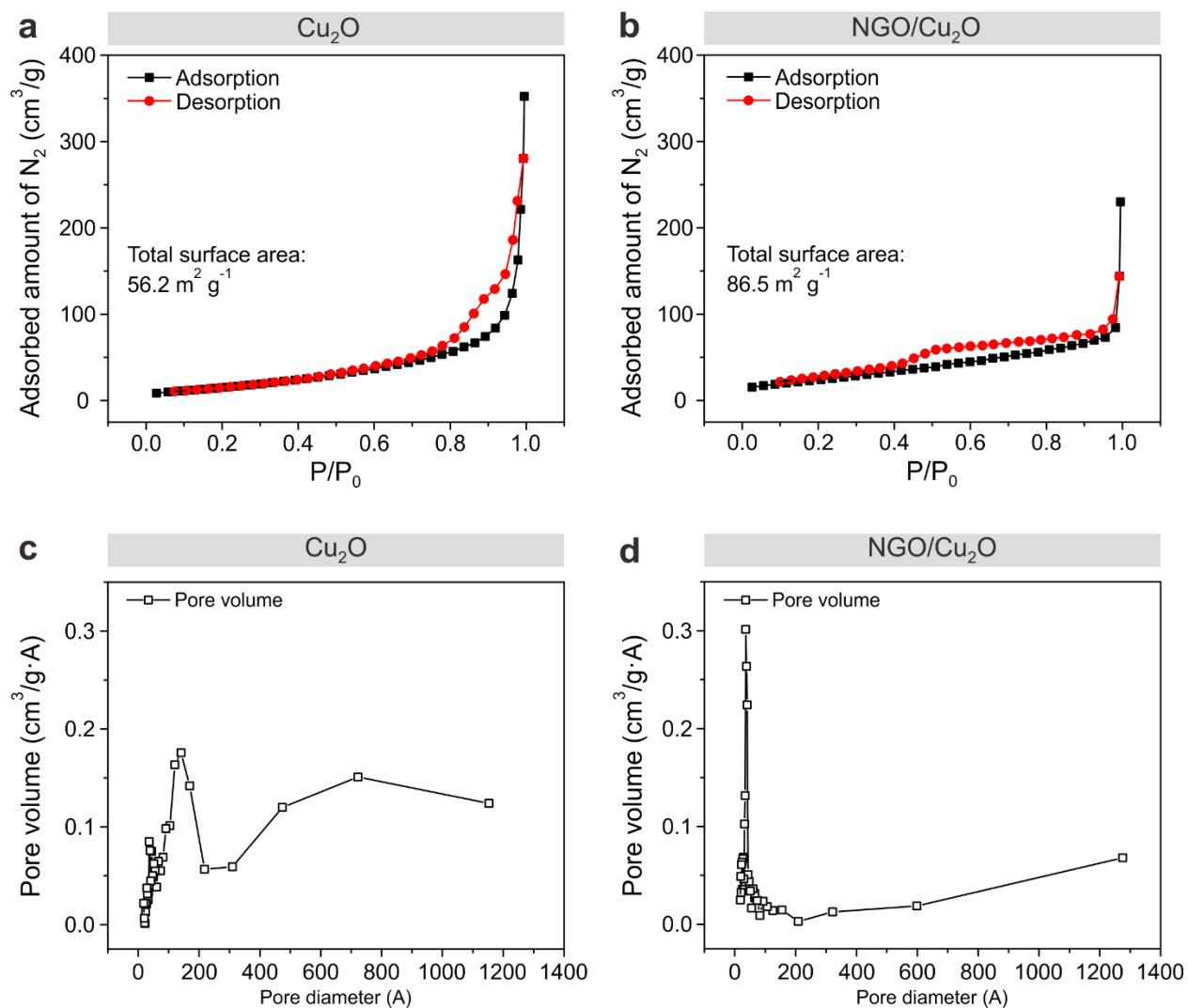


**Figure S3.** Nitrogen adsorption-desorption isotherms of (a) bare Cu<sub>2</sub>O SPs and (b) NGO/Cu<sub>2</sub>O composites and the corresponding pore size distribution plots of (c) bare Cu<sub>2</sub>O SPs and (d) NGO/Cu<sub>2</sub>O nanocomposites.

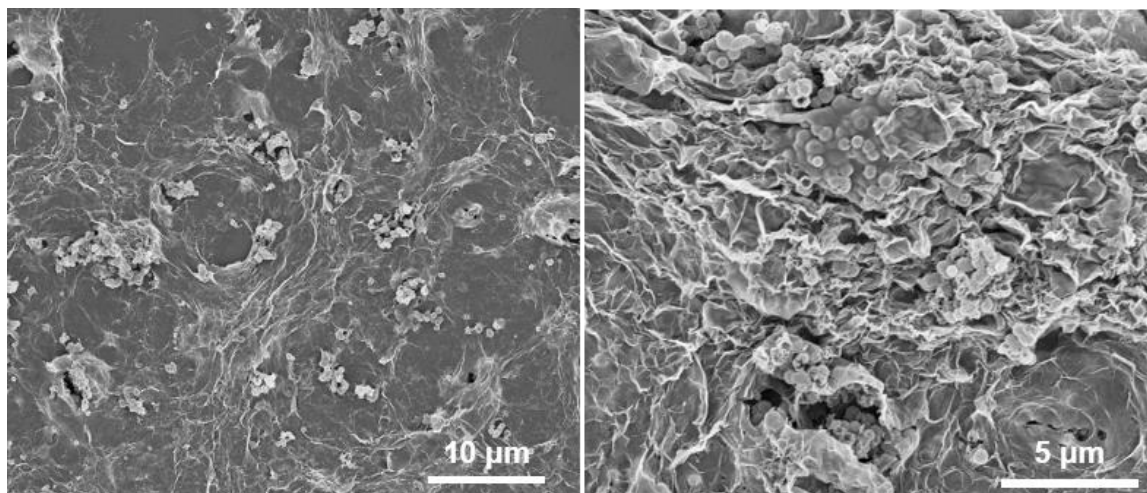


**Figure S4.** SEM images of bulk GO coated Cu<sub>2</sub>O SPs.

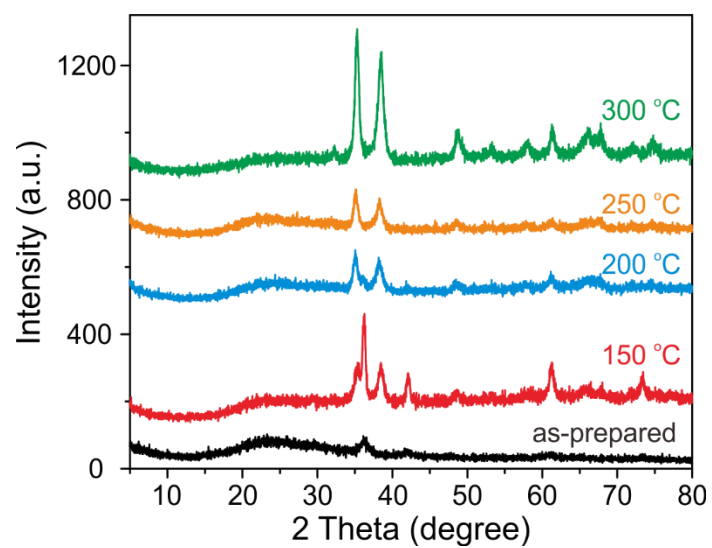


**Figure S5.** XRD of NGO/Cu<sub>2</sub>O composites after thermal treatments at various temperatures.

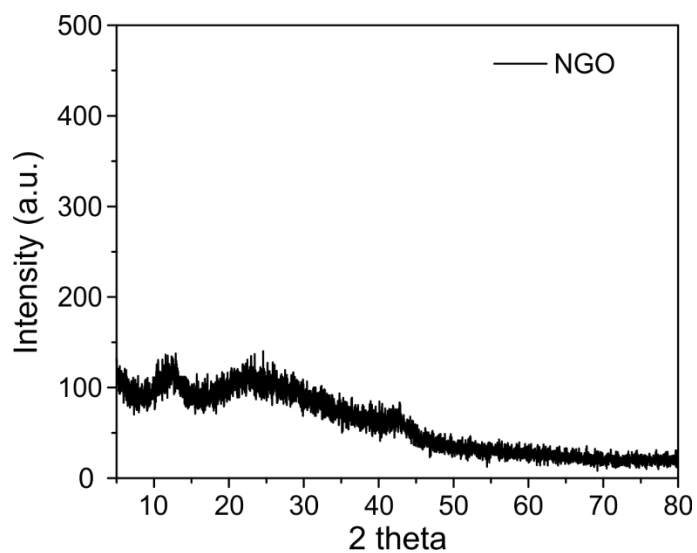


**Figure S6.** XRD of NGO.

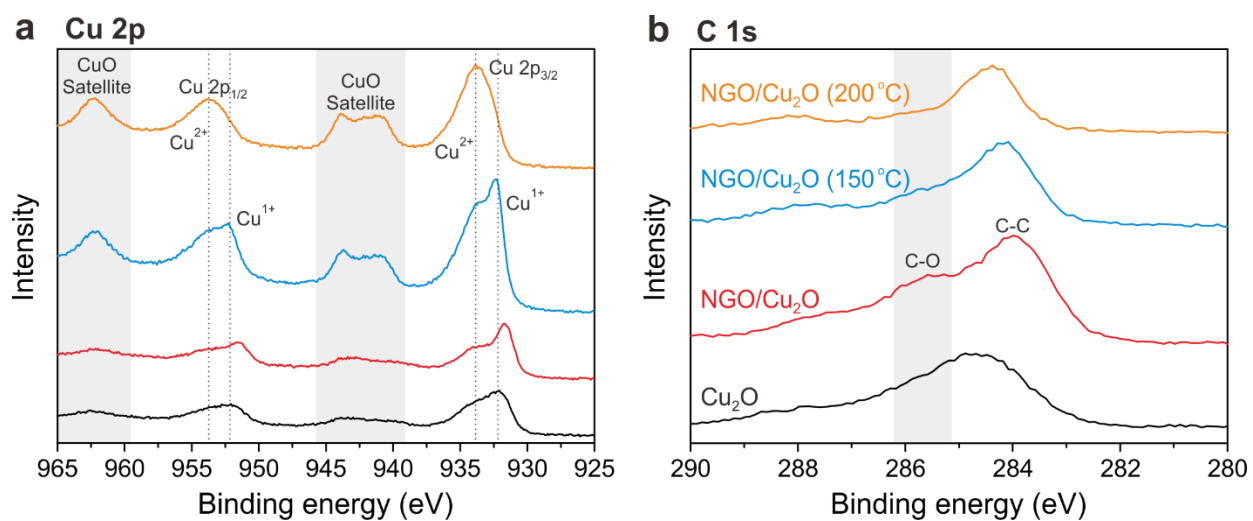


**Figure S7.** High-resolution XPS spectra of (a) Cu 2p and (b) C 1s for Cu<sub>2</sub>O and NGO/Cu<sub>2</sub>O composites after thermal treatment.

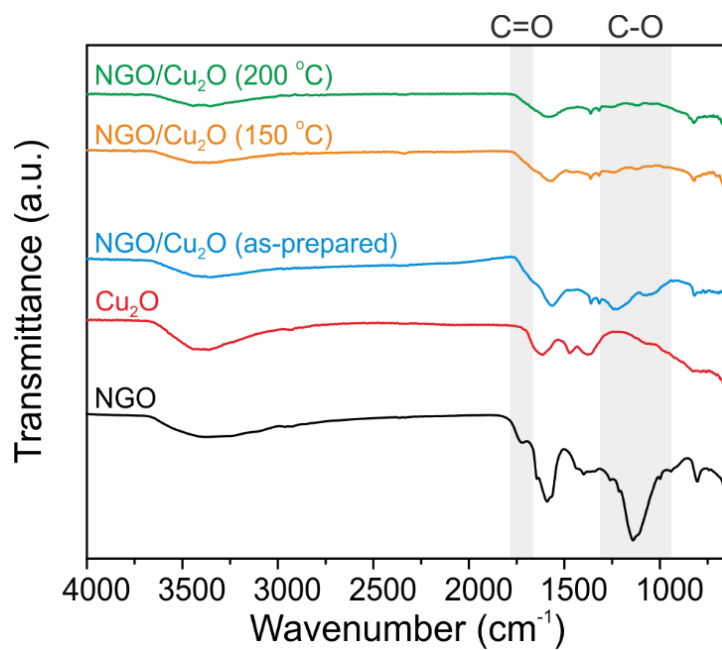


**Figure S8.** FT-IR of NGO/Cu<sub>2</sub>O composites after thermal treatment at various temperatures.

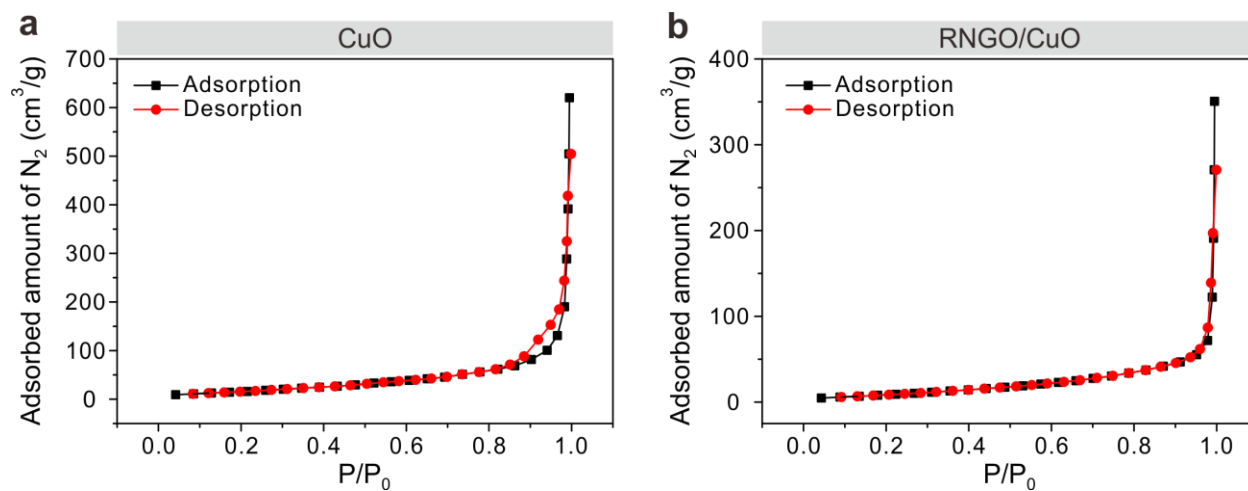


**Figure S9.** Nitrogen adsorption-desorption isotherms of (a) bare CuO SPs and (b) RNGO/CuO composites.

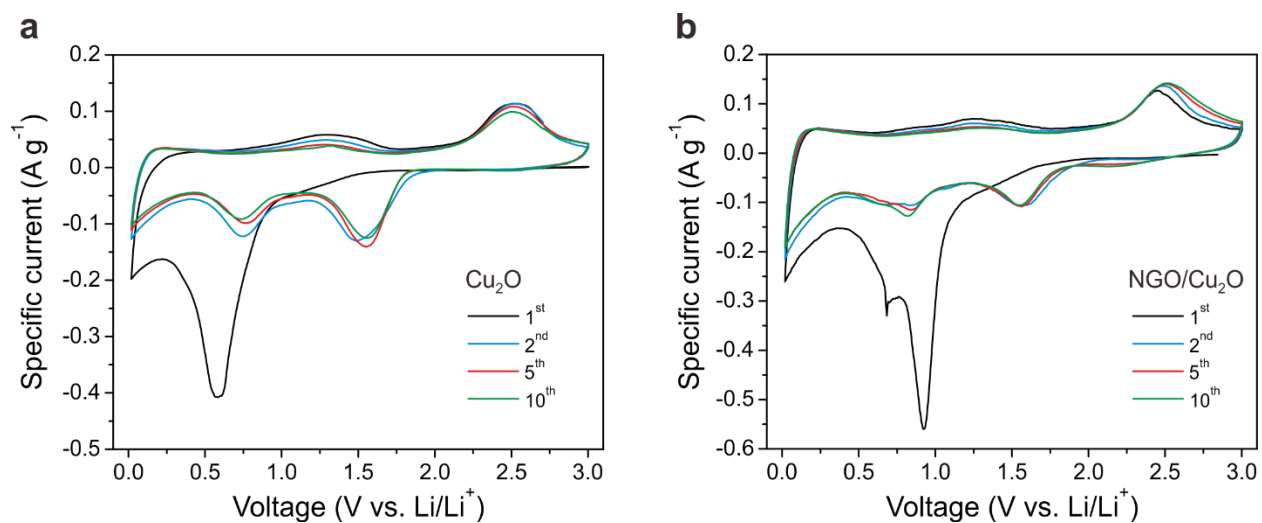


**Figure S10.** CV curves of (a)  $\text{Cu}_2\text{O}$  and (b)  $\text{NGO}/\text{Cu}_2\text{O}$  at various cycles.

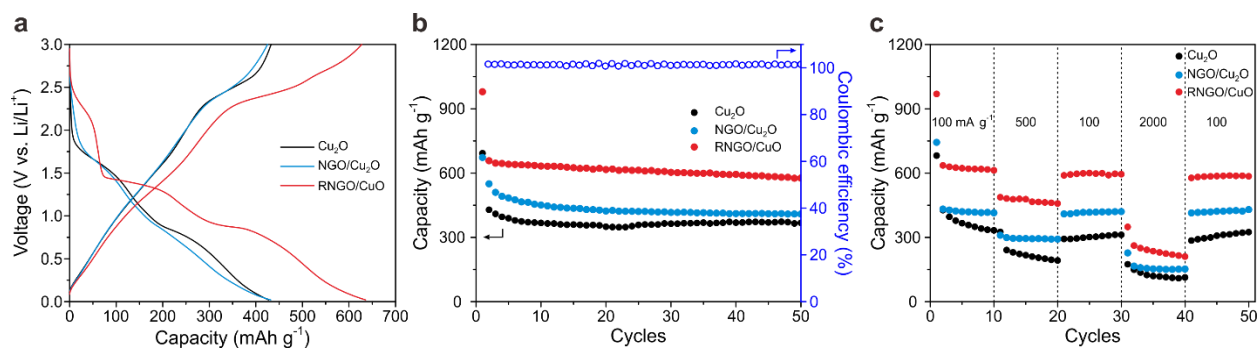


**Figure S11.** (a) Galvanostatic charge/discharge voltage profiles of  $\text{Cu}_2\text{O}$ ,  $\text{NGO}/\text{Cu}_2\text{O}$ , and  $\text{RNGO}/\text{CuO}$  SPs for the 2nd cycle at a current rate of  $100 \text{ mA g}^{-1}$  between  $0.02 - 3.0 \text{ V vs. Li/Li}^+$ . (b) Discharge capacities and coulombic efficiency of  $\text{RNGO}/\text{CuO}$  at a current rate of  $100 \text{ mA g}^{-1}$ , and (c) rate capabilities of  $\text{Cu}_2\text{O}$ ,  $\text{NGO}/\text{Cu}_2\text{O}$ , and  $\text{RNGO}/\text{CuO}$  SPs at varying current densities.

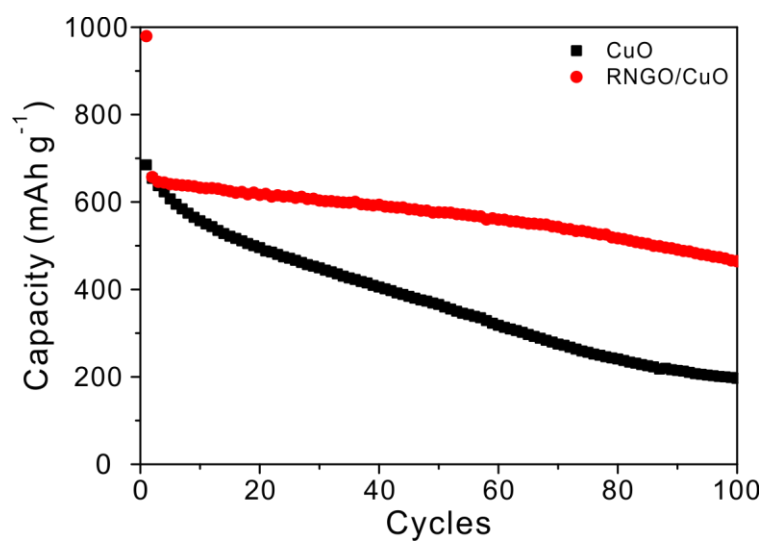


**Figure S12.** Discharge capacities of CuO and RNGO/CuO at a current rate of 100 mA g<sup>-1</sup>.